Mineralogy and Petrology (2006) 86: 45–62
DOI 10.1007/s00710-005-0091-7

Mineralogy and Petrology
Printed in Austria

Zircon geochronology and compositional record of late- to post-kinematic granitoids associated with the Bavarian Pfahl zone (Bavarian Forest)

W. Siebel[1], **M. Thiel**[1], and **F. Chen**[2]

[1] Institut für Geowissenschaften, Universität Tübingen, Tübingen, Germany
[2] Laboratory for Radiogenic Isotope Geochemistry, Institute of Geology and Geophysics, Chinese Academy of Sciences, Beijing, China

Received February 18, 2005; revised version accepted May 22, 2005
Published online August 3, 2005;
Editorial handling: J. Košler

Summary

The northwest-striking Pfahl zone, Bavarian Forest, is a mylonitic shear zone that is associated with brittle-ductile deformation fabrics and a conspicuous hydrothermal quartz mineralization. Two granites from this shear zone yield U–Pb and Pb–Pb evaporation ages between 321–329 Ma and two granodiorites give concordant ^{238}U–^{206}Pb and ^{235}U–^{207}Pb ages of 325 ± 3 Ma and 326 ± 3 Ma, respectively. Zircon populations of the granitoids show sub-types clustering around S_{20}, S_{10} (granite) and S_{22} to S_{24} (granodiorite) testifying different magma affinity. Compositional and isotopic characteristics indicate that the granites and granodiorites were coeval melts, but not differentiates of a single parent magma. The granodiorites were derived from a source with higher time-integrated $^{87}Rb/^{86}Sr$ and lower $^{147}Sm/^{144}Nd$ ratios than the granites. One granite body is transected by the shear zone but the main mass of the granite is largely undeformed. This finding suggests that granite intrusion predates the final stage of ductile deformation along the Pfahl shear zone.

Introduction and geological problem

The Pfahl zone is a late Variscan shear zone in the Moldanubian terrane that forms a major structural feature in the western part of the Bohemian Massif. It has attracted geologists for more than a century, because this zone hosts huge amounts of hydrothermal quartz (e.g. *Ochotzky* and *Sandkühler*, 1914; *Hofmann*, 1962; *Peucker-Ehrenbrink* and *Behr*, 1993) and, given its resistance to weathering, the

quartz forms spectacular cliffs. However, accurate dating of the time and duration of shear activity, deformation and quartz mineralization has been elusive. Recently, zircons from deformed magmatic rocks of intermediate composition (palites of the older literature, *Frentzel*, 1911) have been dated by the U–Pb isotope dilution and Pb–Pb evaporation methods (*Siebel* et al., 2005). These rocks which crop out along the southwestern side of the Pfahl zone, gave ages of 334 ± 3 Ma, 334.5 ± 1.1 Ma (average $^{207}Pb/^{206}Pb$-evaporation ages) and 327–342 Ma (range of U–Pb ages), and this time interval was interpreted as an upper age limit of shear zone activity. In the same study, sheared dikes, which cut the palites, were dated by the U–Pb method at 326–331 Ma. The dikes locally have mylonitic fabrics and their ages place an upper limit for this ductile deformation event. The time of hydrothermal activity is constrained by Rb–Sr dating of pure and acid-leached quartz, for which an age of 247 ± 21 Ma was determined (*Horn* et al., 1986).

The Pfahl zone also played a major role in localizing multiple granitoid intrusions. The granites are largely undeformed and, so far, have not been investigated in detail. Given the fact that the granites intruded the Pfahl zone, their age can provide further time constraints on the shear zone activity. In this study, we have investigated two granite bodies and associated granodiorites of the Pfahl zone. Zircon geochronological work is complemented by zircon typological studies, geochemical and Sr–Nd isotope analyses. Emphasis is also placed on the genetic relation between the granodiorites and granites.

Field description and petrography

The two investigated granite bodies occur in the central segment of the Bavarian Pfahl near the town of Regen (Fig. 1). One of them, hereafter referred to as the Rinchnach granite, closely bounds the northeast side of the Pfahl zone and crops out opposite to the zone of palites and foliated granitoids. In contrast to the palites the Rinchnach granite is largely undeformed. Another undeformed granite body occurs 20 km further to the northwest. This granite, termed Patersdorf granite, occupies both sides of the Pfahl zone. The mylonitic shear zone cuts the granite into two parts. Within the granite, the shear zone is narrower (less than 500 m) than elsewhere in the Pfahl zone (*Ott*, 1983). The localization of deformation into a central zone is consistent with emplacement of the Patersdorf granite after the major stage of penetrative shear deformation along the Pfahl zone.

Both granites host several active quarries where macroscopically fresh samples are available. In the Wildtier quarry (for location see Fig. 1), the granite is in contact with two dark facies of biotite-granodiorite, a fine- to medium-grained variety and a coarse-grained variety. This quarry which provides excellent exposure of the contacts between the intrusions shows that the coarse-grained granodiorite facies intruded the fine-grained facies. The granodiorites are part of a larger body that can be traced for several km towards northwest (*Ott*, 1983 and Fig. 1). The granodiorites are generally massive, but locally they are deformed and have a magmatic/tectonic foliation. This fabric appears to be directly related to the emplacement of the pluton in an existing and active fault zone. Outcrop relationships within the Wildtier quarry further indicate that both types of granodiorites

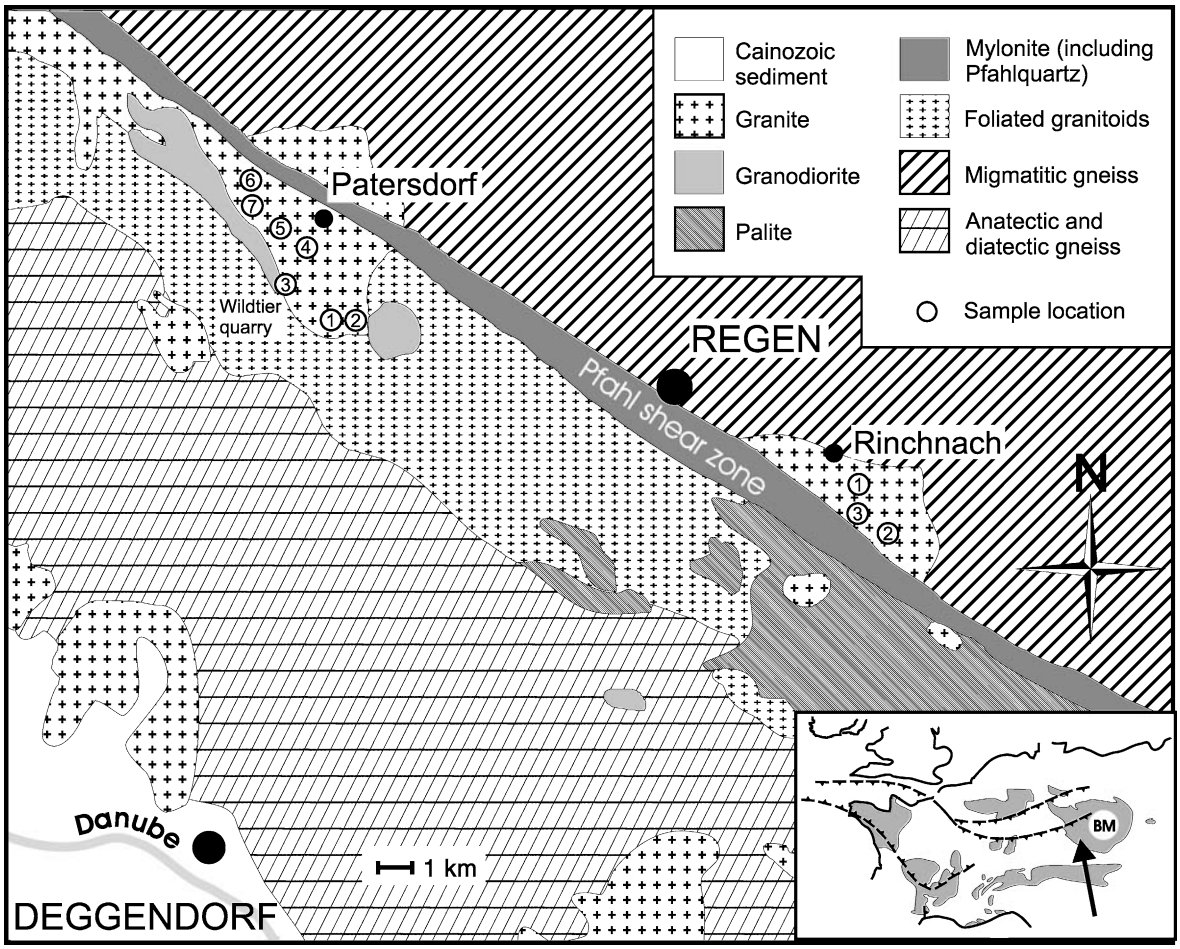

Fig. 1. Simplified geological map of the Bavarian Forest (based on maps published by *Troll*, 1967 and *Ott*, 1983) showing the distribution of late-Variscan magmatic rocks and sample locations. Collected granodiorite samples are from the Wildtier quarry (location Patersdorf 3). Note that migmatites (generally cordierite-bearing) are more abundant northeast of the Pfahl zone whereas in the southwest various types of anatectic gneisses are the dominant rock type. Inset shows the location of the study area within the European Variscan fold belt (*BM* Bohemian Massif)

predated the granites. Material which macroscopically resemble the granodiorites occur in nodules or rafts as microgranular enclaves within the Patersdorf granite.

The granodiorites consist of quartz, K-feldspar, plagioclase (oligoclase-andesine) and biotite. The coarse-grained granodiorite contains isolated large K-feldspar porphyrocrysts (3–5 cm long) for which recently a Rb–Sr single crystal age of 308 ± 5 Ma was obtained (*Siebel* et al., unpublished data). Accessory primary phases include zircon, apatite, titanite and opaques. The Rinchnach and Patersdorf granites possess textural and mineralogical similarities. Both granites have fine-grained equigranular textures. Their modal composition is remarkably constant and they are composed of quartz, K-feldspar, plagioclase, typically oligoclase, and biotite with accessory zircon, apatite and opaques. The large amount of hydrothermal

fluids, which have been expelled tectonically in the Pfahl zone gave rise to alteration of the granitoids. Although our samples are macroscopically fresh, sericitization of the feldspar is often observed under the microscope and typically, biotite is partially replaced by pale-green chlorite and the released Ti has combined with Ca to form secondary titanite.

Analytical procedures

Major and trace element concentrations were determined using X-ray fluorescence (XRF) spectrometry on fused glass beads from whole-rock powder. Measurements were preformed on a Bruker AXS S4 Pioneer spectrometer by standard analytical techniques as described in *Potts* and *Webb* (1992). The internal structure (growth zoning) of zircons was studied by cathodoluminescence (*Vavra*, 1990) using a JEOL JXA-8900RL electron-microprobe, and, for sample PaDr1, a cold cathodoluminescence stage (Technosyn, Model 8200 Mk4) in combination with a petrographic microscope. The typology of zircons was determined according to the scheme of *Pupin* (1980).

For Rb–Sr and Sm–Nd isotope analyses ^{87}Rb–^{84}Sr and ^{149}Sm–^{150}Nd spikes were added to the sample powders. After digestion, Rb, Sr, Sm and Nd were isolated by ion exchange chromatography and all isotopic measurements were made in static TIMS measurement on a Finnigan MAT 262 mass spectrometer at the University of Tübingen. The $^{87}Sr/^{86}Sr$ and $^{143}Nd/^{144}Nd$ isotope ratios were normalized to $^{86}Sr/^{88}Sr = 0.1194$ and to $^{146}Nd/^{144}Nd = 0.7219$, respectively. Total procedural blanks (chemistry and loading) were <160 pg for Sr and <80 pg for Nd. Twelve analyses of the LaJolla Nd standard made during the course of analyses have a mean value of $^{143}Nd/^{144}Nd = 0.511830 \pm 0.000007$. Within the same period, the NBS 987 Sr standard yielded a $^{87}Sr/^{86}Sr$ ratio of 0.710252 ± 0.000012 ($n = 17$). Analytical techniques for zircon Pb-evaporation (*Kober*, 1986, 1987) are described in *Siebel* et al. (2005). The U–Pb zircon analyses were carried out by standard isotope dilution methods as described in *Chen* and *Siebel* (2004). Zircon fractions were less than 0.05 mg in weight (Table 3), and the total procedural blank was 7 pg. The U–Pb age calculations were done by the PBDAT program (*Ludwig*, 1993) and the fitting of the discordia lines using Isoplot/Ex (*Ludwig*, 2003).

Geochemical and isotopic composition

The studied granites are metaluminous to moderately peraluminous, (A/CNK: 0.99–1.03), with SiO_2 contents between 67 and 70 wt.% (Table 1). The whole-rock geochemical data show a narrow range of compositions marked by a slight decrease in Al_2O_3, TiO_2, Fe_2O_3tot, CaO, MgO, P_2O_5, Ba and Sr and increase of K_2O and Rb with rising SiO_2. The samples from the two granodiorites are metaluminous (A/CNK: 0.95 and 0.96), with SiO_2 contents at 62 and 65 wt.%. Most of the major elements of the granodiorites differ in abundance from the range found in the granites. The granodiorites also have higher Ba, Zr, Ce, Nd, Sm and Y concentration compared to the granites.

Table 1. *Chemical composition of whole-rock samples from granodiorites (PaDr1 – fine grained variety, PaDr2 – coarse-grained variety) and granites (Pa – Patersdorf, Ri – Rinchnach). Major elements in wt%, trace elements in parts per million (ppm). Concentrations for Rb, Sr, Sm and Nd were determined by the isotope dilution method all others elements by XRF*

Sample	PaDr1	PaDr2	Pa1	Pa2	Pa3	Pa4	Pa5	Pa6	Pa7	Ri1	Ri2	Ri3
SiO_2	65.40	62.44	69.38	68.53	67.52	68.35	68.78	68.98	70.19	67.12	70.01	68.32
TiO_2	1.16	1.20	0.49	0.50	0.53	0.52	0.51	0.53	0.47	0.58	0.48	0.48
Al_2O_3	14.53	16.36	15.28	15.08	15.28	14.94	15.56	15.43	15.13	16.46	15.00	15.09
Fe_2O_3	4.98	6.03	2.90	2.95	3.08	3.07	3.04	3.12	2.70	3.57	2.90	2.80
MnO	0.07	0.09	0.05	0.05	0.05	0.05	0.05	0.05	0.04	0.06	0.05	0.05
MgO	1.31	1.96	1.02	1.02	1.09	1.10	1.09	1.14	0.91	1.32	1.00	0.96
CaO	2.49	3.78	2.37	2.38	2.61	2.48	2.69	2.73	2.18	3.39	2.40	2.34
Na_2O	3.10	3.41	3.55	3.55	3.67	3.46	3.71	3.72	3.66	3.88	3.53	3.59
K_2O	5.11	4.39	4.32	4.39	4.29	4.18	4.32	4.05	4.55	3.20	4.37	4.45
P_2O_5	0.46	0.43	0.19	0.18	0.21	0.19	0.18	0.18	0.18	0.20	0.17	0.19
LOI	0.72	0.69	0.77	0.63	0.61	0.82	0.76	0.77	0.57	0.50	0.66	0.59
Total	99.32	100.76	100.33	99.26	98.94	99.16	100.69	100.70	100.58	100.28	100.57	98.86
Ba	1159	1335	857	897	960	808	856	820	847	908	771	794
Rb	176	140	178	181	180	170	194	196	207	136	189	182
Sr	201	329	282	273	314	285	324	333	301	379	274	266
Zr	655	595	261	263	282	273	261	285	263	210	194	247
Y	67	52	38	40	43	38	41	44	37	25	28	42
Ce	162	182	99	81	100	86	98	108	101	84	71	84
Nd	78.9	77.0	37.6	35.7	44.3	26.6	–	–	–	30.9	35.8	36.6
Sm	14.55	13.45	6.85	6.56	7.91	5.44	–	–	–	5.87	7.10	6.75
A/CNK	0.96	0.95	1.03	1.01	0.99	1.01	0.99	1.00	1.01	1.03	1.01	1.01

– Not determined, *LOI* Loss on Ignition, *A/CNK* molecular $[Al_2O_3/(CaO + Na_2O + K_2O)]$

The Sr isotopic study (Table 2) reveals initial $^{87}Sr/^{86}Sr$ ratios (325 Ma) of 0.7060–0.7071 for Rinchnach and Patersdorf granites and significantly higher Sr ratios of 0.7081 and 0.7086 for the two granodiorites. The εNd (325 Ma) values are in a narrow range between −4.3 and −4.8 for the granites and at −5.3 for the granodiorites. The Nd model ages (1.3–1.4 Ga, according to the depleted mantle model) indicate that recycled Precambrian material is present in all granitoids.

Zircon morphology/typology and geochronology

Zircons from the granitoids are subhedral to euhedral in shape. The zircon population from the granodiorites is dominantly translucent to transparent whereas the granite samples mainly yielded brownish dull crystals. In all of the investigated zircon grains the intensity of the cathodoluminescence signal shows major variations (Fig. 2). In most cases this is caused by oscillatory zoning pattern which reflects alternating uptake of trace elements during crystal growth (e.g., *Hanchar* and *Miller*, 1993; *Hanchar* and *Rudnick*, 1995; *Corfu* et al., 2003; *Nasdala* et al., 2003). Many zircons show evidence of complicated growth histories in the form of complex zoning patterns, inherited inner cores and overgrowths (e.g., Ri1: grain 5,

Table 2. *Rb–Sr and Sm–Nd analytical data together with εNd values and T_{DM} model ages for selected samples from the Pfahl granitoids. For sample description and Rb, Sr, Sm, Nd concentrations see Table 1*

Sample	$^{87}Rb/^{86}Sr$	$^{87}Sr/^{86}Sr$[1]	$(^{87}Sr/^{86}Sr)_i$[2]	$^{147}Sm/^{144}Nd$	$^{143}Nd/^{144}Nd$[1]	$(^{143}Nd/^{144}Nd)_i$[2]	$\varepsilon Nd_{(t)}$[3]	T_{DM}(Ga)[4]
PaDr1	2.535	0.719796 ± 7	0.70807	0.1114	0.512183 ± 9	0.511946	−5.3	1.37
PaDr2	1.235	0.714356 ± 10	0.70864	0.1055	0.512175 ± 7	0.511951	−5.3	1.31
Pa1	1.826	0.715206 ± 7	0.70676	0.1103	0.512225 ± 10	0.511990	−4.5	1.30
Pa2	1.926	0.715648 ± 8	0.70674	0.1109	0.512229 ± 8	0.511993	−4.4	1.30
Pa3	1.665	0.714411 ± 10	0.70671	0.1080	0.512215 ± 8	0.511985	−4.6	1.28
Pa4	1.726	0.715054 ± 11	0.70707	0.1236	0.512260 ± 9	0.511997	−4.3	1.42
Ri1	1.038	0.710797 ± 10	0.70599	0.1148	0.512244 ± 9	0.512000	−4.3	1.33
Ri2	1.996	0.716075 ± 9	0.70684	0.1199	0.512228 ± 8	0.511973	−4.8	1.42
Ri3	1.982	0.715928 ± 9	0.70676	0.1116	0.512212 ± 9	0.511975	−4.8	1.33

[1] Errors are $2\sigma_{measured}$; [2] initial ratios calculated using the age 325 Ma; [3] typical uncertainty in $\varepsilon Nd_{(t)}$ ($t = 325$ Ma) is ± 0.4; [4] Nd depleted mantle model age (two-stage) with parameters given in *Liew* and *Hofmann* (1988)

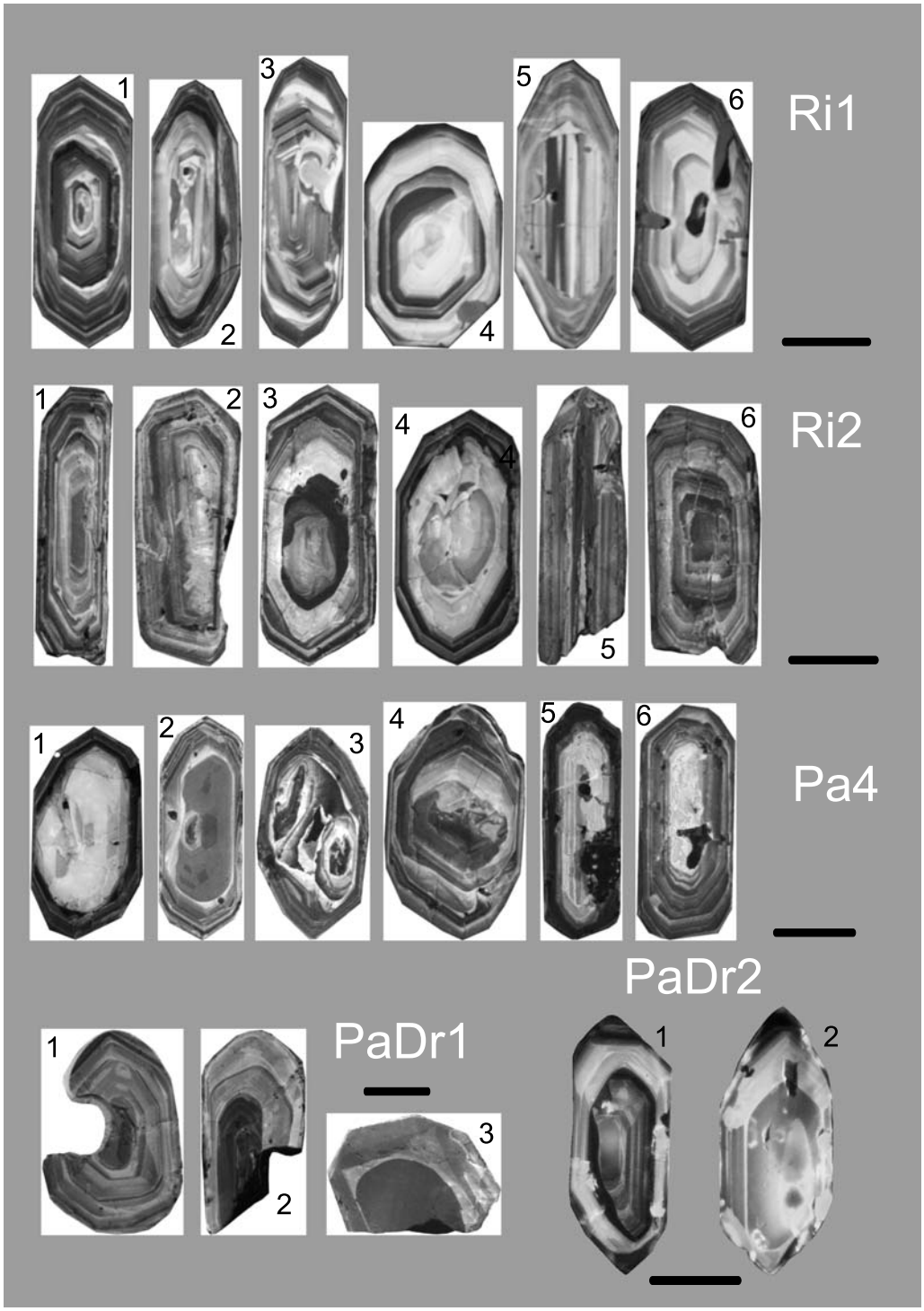

Fig. 2. Cathodoluminescence images of sectioned zircon from granites (samples Ri and Pa) and granodiorites (samples PaDr). Scale bars 40 μm

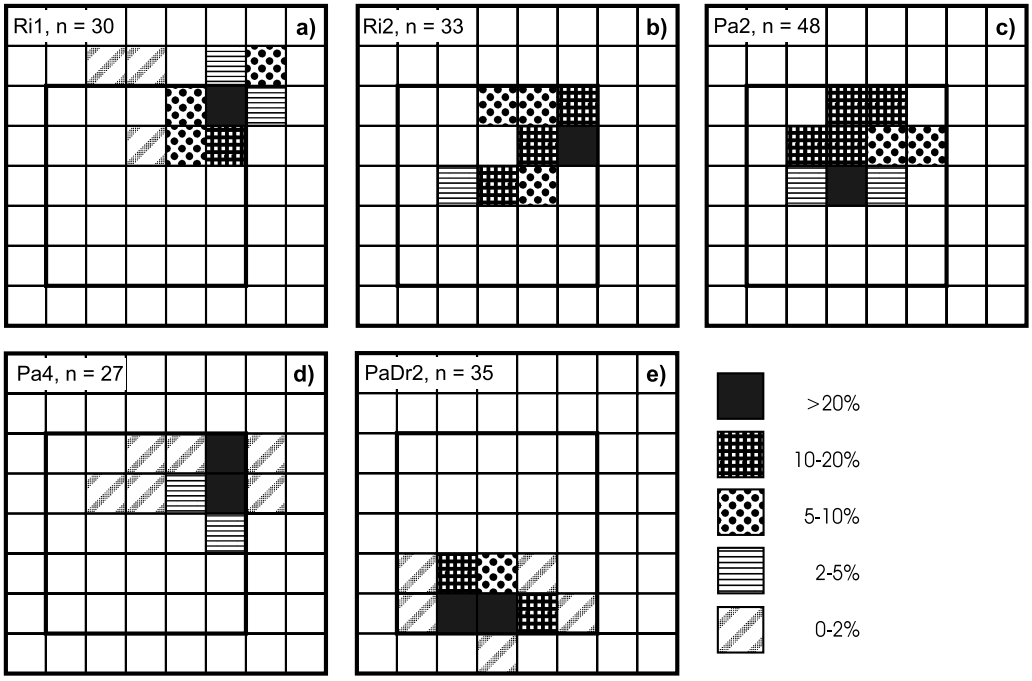

Fig. 3. Frequency distribution of zircon morphology (according to *Pupin*, 1980) for granites (**a**–**d**) and granodiorite PaDr2 (**e**) of the present study. Zircon material in sample PaDr1 was not sufficient for evaluation. *n* number of zircon grains which were used for statistical evaluation

Ri2: grains 3 and 4, Pa4: grains 1 and 2) or inclusions of smaller zircons (Pa4: grain 3). The exact percentage of zircons with cores is difficult to determine because of the internal resorption and corrosion features which are particularly obvious in samples Pa4 and PaDr2. Irregular shaped areas as seen in PaDr1 (grain 1) may also reflect resorption.

In the *Pupin* diagram (*Pupin*, 1980), which shows the distribution of the external crystal faces, two maxima can be observed, one for the granites, one for the granodiorite (Fig. 3). For the granites the most common types are S_{3-10} and S_{13} with a maximum at S_{10}. Among the zircons from the investigated granodiorite sample euhedral transparent crystals predominate (mostly S_{17}, S_{22}, S_{23} and S_{24} forms).

In order to determine the zircon ages we used the Pb–Pb evaporation and the U–Pb isotope dilution methods. For U–Pb analyses about half of the fractions were mechanically abraded according to the method of *Krogh* (1982) and the abrasion time is given in Table 3. Sample PaDr1 contains two fractions with pre-Carboniferous apparent U–Pb ages. One is concordant at 401 Ma whereas the other fraction is discordant and gives a $^{207}Pb/^{206}Pb$ age around 402 Ma (Table 3). Another fraction from sample PaDr2 gives a slightly lower concordant age of 314 Ma and this could be caused by later Pb loss. The remaining zircon fractions from the two granodiorites are almost concordant with very similar $^{207}Pb/^{235}U$ and $^{206}Pb/^{238}U$ U ages (Fig. 4, Table 3). From these fractions, $^{206}Pb/^{238}U$ and $^{207}Pb/^{235}U$ mean ages of 325 ± 3 Ma and 326 ± 3 Ma are obtained which probably provide the best estimate for the time of emplacement and crystallization. The narrow range of age

Table 3. *U–Pb isotope dilution data for zircons from Rinchnach and Patersdorf granitoids*

Sample/ fraction[1]	Abrasion time (h)	Weight[2] (mg)	$^{206}Pb^{3}/^{204}Pb$	U^{2} (ppm)	Pb^{2} (ppm)	Th/U^{4}	Isotopic ratios[5]			Calculated ages (Ma)			% Disc.[6]
							$^{206}Pb/^{238}U$	$^{207}Pb/^{235}U$	$^{207}Pb/^{206}Pb$	$^{206}Pb/^{238}U$	$^{207}Pb/^{235}U$	$^{207}Pb/^{206}Pb$	
PaDr1-1	–	0.016	418	389	24	0.26	0.05452 ± 45	0.4116 ± 54	0.05475 ± 55	342	350	402	15.3
PaDr1-2	–	0.019	775	613	35	0.47	0.05175 ± 33	0.3777 ± 31	0.05294 ± 27	325	325	326	0.2
PaDr1-3	–	0.025	897	467	27	0.61	0.05209 ± 39	0.3801 ± 46	0.05293 ± 48	327	327	326	−0.4
PaDr1-4	–	0.020	493	289	21	0.37	0.06412 ± 64	0.4850 ± 63	0.05486 ± 40	401	401	407	1.6
PaDr2-1	27	0.025	1562	455	24	0.34	0.05177 ± 43	0.3768 ± 53	0.05278 ± 57	325	325	319	−2.1
PaDr2-2	27	0.025	1049	245	13	0.36	0.05171 ± 51	0.3761 ± 84	0.05275 ± 99	325	324	318	−2.3
PaDr2-3	27	0.039	1044	313	17	0.25	0.05221 ± 29	0.3834 ± 24	0.05326 ± 15	328	330	340	3.6
PaDr2-4	27	0.026	480	218	13	0.57	0.05115 ± 30	0.3773 ± 44	0.05349 ± 52	322	325	350	8.0
PaDr2-5	27	0.022	1583	215	11	0.36	0.04995 ± 41	0.3625 ± 86	0.0526 ± 11	314	314	313	−0.4
PaDr2-6	27	0.017	548	174	10	0.46	0.05118 ± 36	0.3783 ± 78	0.05361 ± 99	322	326	355	9.6
PaDr2-7	27	0.006	82	164	17	0.49	0.05246 ± 59	0.384 ± 20	0.0531 ± 26	330	330	332	0.7
Ri1-1	–	–	5214	–	–	0.40	0.04618 ± 25	0.3361 ± 19	0.052789 ± 69	291	294	320	9.3
Ri1-2	–	–	5151	–	–	0.39	0.04423 ± 31	0.3211 ± 23	0.052642 ± 83	279	283	313	11.1
Ri1-3	–	–	3009	–	–	0.38	0.04250 ± 32	0.3082 ± 23	0.052601 ± 63	268	273	312	14.3
Ri1-4	–	–	1259	–	–	0.42	0.04439 ± 22	0.3212 ± 16	0.052468 ± 39	280	283	306	8.7
Ri1-5	–	–	3844	–	–	0.40	0.04125 ± 21	0.2984 ± 16	0.052466 ± 84	261	265	306	15.2
Ri1-6	5.5	0.025	2215	889	44	0.42	0.04743 ± 34	0.3441 ± 26	0.05262 ± 14	299	300	312	4.3
Ri1-7	5.5	0.020	549	954	50	0.49	0.04580 ± 28	0.3361 ± 25	0.05322 ± 20	289	294	338	14.9
Ri1-8	5.5	0.022	1826	1113	51	0.38	0.04443 ± 29	0.3234 ± 23	0.05279 ± 15	280	285	320	12.7
Ri1-9	5.5	0.024	887	1188	57	0.34	0.04515 ± 25	0.3287 ± 20	0.05281 ± 13	285	289	321	11.6
Ri2-1	5	0.019	778	1755	96	0.46	0.04980 ± 45	0.3476 ± 40	0.05256 ± 34	313	313	310	−3.3
Ri2-2	5	0.013	1074	2417	122	0.18	0.04994 ± 40	0.3643 ± 31	0.05291 ± 12	314	315	325	3.4
Ri2-3	5	0.014	1053	1569	75	0.26	0.04614 ± 29	0.3359 ± 24	0.05280 ± 16	291	294	320	9.3
Ri2-4	5	0.028	3815	1311	70	0.29	0.05382 ± 39	0.3907 ± 29	0.052658 ± 87	338	335	314	−7.8

(*continued*)

Table 3 (*continued*)

Sample/ fraction[1]	Abrasion time (h)	Weight[2] (mg)	$^{206}Pb^{3}/^{204}Pb$	U[2] (ppm)	Pb[2] (ppm)	Th/U[4]	Isotopic ratios[5]			Calculated ages (Ma)			% Disc.[6]
							$^{206}Pb/^{238}U$	$^{207}Pb/^{235}U$	$^{207}Pb/^{206}Pb$	$^{206}Pb/^{238}U$	$^{207}Pb/^{235}U$	$^{207}Pb/^{206}Pb$	
Ri2-5	5	0.072	452	1608	87	0.26	0.04833 ± 47	0.3546 ± 35	0.053201 ± 85	304	308	337	9.9
Pa2-1	–	0.019	401	758	51	0.76	0.05303 ± 47	0.3865 ± 55	0.05286 ± 58	333	332	323	−3.2
Pa2-2	–	0.038	920	683	35	0.28	0.04865 ± 27	0.3534 ± 26	0.05268 ± 24	306	307	315	2.8
Pa2-3	–	0.024	732	1081	56	0.16	0.05032 ± 35	0.3657 ± 29	0.05271 ± 21	317	317	316	−0.2
Pa2-4	–	0.032	406	7621	153	0.48	0.01681 ± 17	0.1227 ± 12	0.052950 ± 94	107	118	327	67.7
Pa4-1	–	0.026	2577	1023	49	0.33	0.04680 ± 42	0.3404 ± 32	0.05274 ± 15	295	297	318	7.5
Pa4-2	–	0.006	2096	1879	131	0.23	0.06925 ± 37	0.7216 ± 44	0.07557 ± 20	432	552	1084	62.2
Pa4-3	–	0.023	2447	2185	99	0.38	0.04402 ± 25	0.3190 ± 19	0.052563 ± 73	278	281	310	10.6
Pa4-4	–	0.025	6497	1657	76	0.21	0.04731 ± 26	0.3450 ± 21	0.05289 ± 15	298	301	324	8.2
Pa4-5	–	0.028	4284	1396	58	0.20	0.04308 ± 23	0.3119 ± 20	0.05251 ± 17	272	276	308	12.0
Pa4-6	8	0.032	1146	317	19	0.20	0.05693 ± 34	0.4257 ± 34	0.05423 ± 28	357	360	381	6.5
Pa4-7	2	0.027	1064	667	31	0.40	0.04466 ± 45	0.3210 ± 53	0.05213 ± 68	282	283	291	3.3
Pa4-8	2	0.043	1690	590	28	0.47	0.04524 ± 58	0.3289 ± 44	0.05273 ± 23	285	289	317	10.2
Pa4-9	2	0.033	1457	557	30	0.37	0.05104 ± 37	0.3744 ± 31	0.05319 ± 21	321	323	337	4.9

[1] All zircon fractions. [2] Weight and concentration error better than 20%. [3] Measured ratio corrected for mass discrimination and spike contribution. [4] Th/U model ratio calculated from $^{208}Pb/^{206}Pb$ ratio and age of the sample. [5] Corrected for blank Pb, U, and initial common Pb based on the *Stacey* and *Kramers* (1975) model; errors are $2\sigma_m$. [6] Degree of discordance (%) for the given $^{207}Pb/^{206}Pb$ age of the fraction

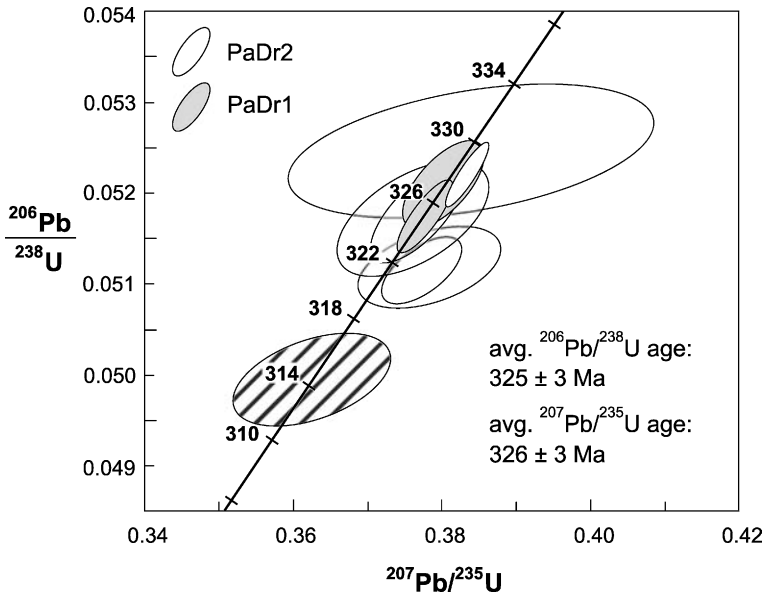

Fig. 4. U–Pb concordia diagram for zircon fractions from the granodiorites. Hatched ellipse indicates fraction from PaDr2 (coarse-grained variety) which was excluded from mean age calculation. Error ellipses are 2σ

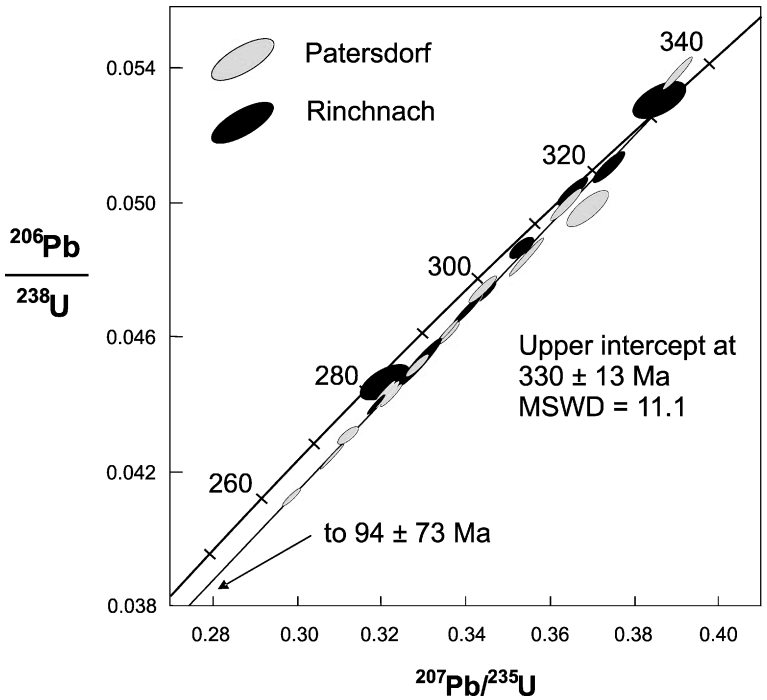

Fig. 5. U–Pb concordia diagram for zircon fractions from the Patersdorf and Rinchnach granite. Two fractions with inherited cores (Pa4-2, Pa4-6, Table 3) plot outside the range of the diagram and were excluded from the discordia fit. One fraction which suffered very strong loss of Pb (Pa2-4) plots also outside this diagram but was included in the discordia line fit. Data-point error ellipses are 2σ

values in most of the zircon fractions is interpreted as representing an almost synchronous emplacement of the fine- and the coarse-grained granodiorite.

The granite zircon fractions have higher U and Pb concentrations but similar Th/U ratios than those from the granodiorites (Table 3). Only two out of 27 fractions have significantly older U–Pb apparent ages (Pa4-2 and Pa4-6). The older age data can be explained by the presence of older cores within these fractions possibly inherited from the crust. In detail, these two dates are difficult to interpret due to complexities associated with mixing of inherited and newly grown zircon components as well as later loss of Pb (see below). Most of the remaining granite fractions are variably discordant forming a slightly scattered array pointing towards the origin of the concordia diagram (Fig. 5). The most likely explanation for this pattern is Pb removal either continuously or during a recent uplift or weathering process. No well defined discordia line can be calculated from the different zircon fractions of the four investigated samples. In the concordia diagram there is no difference between the data points from Rinchnach and Patersdorf. If the fractions

Table 4. *$^{207}Pb/^{206}Pb$ evaporation data for single zircons from Rinchnach and Patersdorf granitoids*

Sample	n[1]	$^{204}Pb/^{206}Pb$	$^{206}Pb/^{208}Pb$	Th/U[2]	$^{207}Pb/^{206}Pb$[3]	Age (Ma)	Error[4]
Ri1_1	288	0.000033	8.9	0.36	0.052982 ± 0.000033	328.1	2.7
Ri1_2	108	0.000021	10.1	0.32	0.053045 ± 0.000087	330.7	4.4
Ri1_3	123	0.000173	11.5	0.29	0.053048 ± 0.000103	330.9	5.0
Weighted avg.						**329.2**	**2.1**
Ri2_1	105	0.000166	10.0	0.31	0.052960 ± 0.000093	327.1	4.6
Ri2_2	153	0.000020	14.0	0.23	0.052762 ± 0.000035	318.6	2.7
Ri2_3	226	0.000244	10.1	0.32	0.052715 ± 0.000041	316.6	2.9
Ri2_4	193	0.000324	7.0	0.45	0.052872 ± 0.000039	323.3	2.8
Ri2_4_Far[5]	114	0.000107	7.6	0.42	0.052926 ± 0.000058	325.7	2.5
Weighted avg.						**320.4**	**6.5**
Pa2_1	104	0.000092	6.9	0.48	0.052774 ± 0.000063	319.1	3.6
Pa2_2	297	0.000063	11.6	0.28	0.052790 ± 0.000054	319.8	3.3
Pa2_3	202	0.000071	17.0	0.20	0.052928 ± 0.000057	325.7	3.4
Weighted avg.						**322.0**	**2.0**
Pa4_1	169	0.000020	2.5	2.25	0.052815 ± 0.000061	320.9	3.5
Pa4_2	180	0.000014	6.9	0.45	0.052907 ± 0.000040	324.8	2.9
Pa4_3	403	0.000005	10.3	0.32	0.052847 ± 0.000050	322.3	3.2
Pa4_4	319	0.000010	7.9	0.40	0.052906 ± 0.000051	324.8	3.2
Weighted avg.						**323.4**	**1.6**

[1] Number of measured $^{207}Pb/^{206}Pb$ isotope ratios per grain; [2] model ratio calculated from $^{208}Pb/^{206}Pb$ ratio and age of the sample; [3] errors are $2\sigma_{measured}$; [4] error calculated using following formulae: $\sqrt{(2\sigma/\sqrt{n})^2 + \Delta f^2}$, where n is the number of measured $^{207}Pb/^{206}Pb$ isotope ratios, 2σ is the 2-sigma standard error of the Gaussian frequency distribution function and Δf is an assumed uncertainty of the measured $^{207}Pb/^{206}Pb$ ratio of 0.1%; [5] same grain as Ri2_4 but Pb isotopes measured simultaneously with Faraday cups (not included into weighted average calculation)

from the two granites are combined (excluding the two fractions with inherited components), the isotopic data plot along a regression line giving upper and lower intercept ages of 330 ± 13 Ma and 94 ± 73 Ma, respectively (Fig. 5).

$^{207}Pb/^{206}Pb$ evaporation ages were determined on four samples from the granites (Table 4, Fig. 6). The ages range from 317 to 331 Ma in the Rinchnach granite and from 319 to 326 Ma in the Patersdorf granite with mean ages of 329.2 ± 2.1 Ma

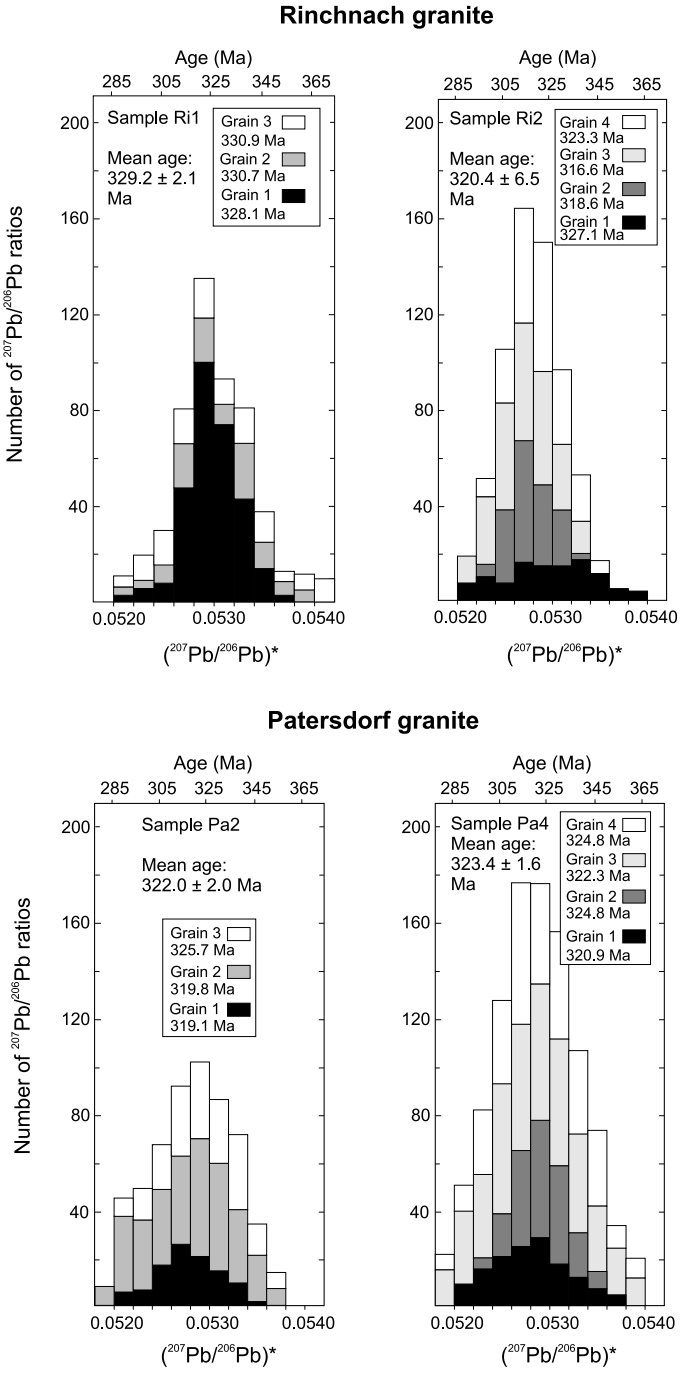

Fig. 6. Histograms showing the frequency distribution of radiogenic $^{207}Pb/^{206}Pb$ ratios obtained from evaporation of zircons from the Rinchnach granite (upper panel) and Patersdorf granite (lower panel)

(sample Ri1, number of analysed grains, n = 3), 320.4 ± 6.5 Ma (Ri2, n = 4), 322.0 ± 2.0 Ma (Pa2, n = 3) and 323.4 ± 1.6 Ma (Pa4, n = 4). Since the cathodoluminescence images indicate a dominantly magmatic origin for most of the grains, we interpret these ages to date the intrusion of the granites. Besides these zircons we found a few zircons with slightly older apparent $^{207}Pb/^{206}Pb$ ages between 330–350 Ma. Such dates were only obtained for the highest temperature evaporation steps and the data are interpreted to record the contribution of Pb from slightly older inherited components.

Discussion

The zircon typological indices I. T and I. A (*Pupin*, 1980) are higher in the granites than in the granodiorites. It has been suggested that temperature and chemistry (*Pupin*, 1980), major and trace element composition (e.g. *Vavra*, 1990, 1994; *Benisek* and *Finger*, 1993), the degree of magma differentiation (*Köhler*, 1970) or $ZrSiO_4$ supersaturation (e.g. *Vavra*, 1990, 1994) are key parameters in the development of zircon prism size relation. The U content of the granite zircons is much higher than in the zircons from the granodiorites (Table 3) reflecting the different melt composition of the two rock types. Thus, compositional effects as well as possible temperature contrasts between the two magmas might have controlled the development of the zircon crystal faces.

From the analytical data it appears that U and probably also Th concentrations have influenced the degree of concordance of the analyzed zircon fractions. The low-U zircons from the granodiorites yield quite concordant results whereas the high-U zircons from the granites clearly suffered various degree of Pb loss. The data in Table 3 also show that abrasion was only moderately successful in increasing the degree of concordance. In the case of sample Pa4, the portion of abraded zircon was probably more enriched in U than the portion left over and the abraded fractions yield slightly less discordant results. The discordant U–Pb systematics of the granites caused by Pb loss precludes a unique age interpretation from the U–Pb data alone. However, the Pb–Pb evaporation ages and the U–Pb ages of the granodiorites show that both granitoids intruded more or less contemporaneously. This finding confirms geochronological result from the northern Oberpfalz (*Siebel* et al., 2003) where intermediate rocks (so-called *redwitzites*) were contemporaneous with the older group of granites. Our data also confirm results from *Söderlund* (1996) and *Karabinos* (1997) that, in case of Pb loss, the intrusion age is better constrained by single-zircon evaporation than by isotope dilution U–Pb analyses.

Cross cutting relationships show that the Patersdorf granite intrudes the granodiorites. Amongst the granodiorites the fine-grained variety preceded the coarse-grained one. Combining field and age data it becomes evident that the granites intruded the granodiorites within a short time interval. The intrusions took place when high-temperature metamorphic conditions prevailed in the Bavarian Forest (*Kalt* et al., 1999, 2000). The contemporaneity of shearing, magmatism, and metamorphism at around ~325 Ma makes it likely that these processes were geodynamically closely related. Other magmatic rocks along the Pfahl zone (palites and foliated granitoids, Fig. 1) are, in general, deformed and were intruded before or during the gneiss-forming event. The Rinchnach and Patersdorf granites are not foliated, but

the latter is truncated by the Pfahl shear zone in its central part. Outside this zone, no high temperature ductile shear fabric was found in the granites. Therefore, we argue that granite emplacement provides a lower age limit for the gneiss-forming event and predates the final stage of ductile deformation along the Pfahl shear zone.

As just noticed, the emplacement of the Rinchnach and Patersdorf granites does not define the end of tectonic processes along the Pfahl zone. After magmatism, temperatures above 650 °C still prevailed at least in shear corridors of the southern area of the Pfahl zone as indicated by quartz microfabrics and a c. 287 Ma ^{40}Ar–^{39}Ar muscovite age (*Brandmayr* et al., 1995). Rb–Sr feldspar ages obtained from the coarse-grained granodiorite of the Wildtier quarry as well as from the palites (*Siebel* et al., unpublished data) mostly fall in the range 290–310 Ma and are linked to late homogenization of the Sr isotopic system caused by the presence of hydrothermal or metamorphic fluids and associated metasomatic processes. The activity of a hydrothermal system in this zone, as manifested by the formation of the huge quartz dike, was dated at 247 ± 21 Ma (*Horn* et al., 1986).

The Paleozoic and Precambrian ages found in some of the zircon fractions reflect inherited zircon domains. From the cathodoluminescence images it can be seen that some of the cores show oscillatory zoning (e.g. Ri1: grain 5, PaDr2: grain 1) indicating that at least some of the cores were inherited from magmatic precursors. The old ages correspond to previously reported Cambrian and Ordovician magmatic events in the Bavarian Forest (*Teipel* et al., 2004). Thus, some of the inherited zircon cores from the Pfahl granitoids might have been derived from remelted Paleozoic granitoids. Constraints for the average crustal residence time of the source material are provided by the 1.3–1.4 Ga whole-rock Nd-model ages. Typically, granitoids from eastern Bavaria have mid-Proterozoic model ages (*Liew* and *Hofmann*, 1988; *Siebel* et al., 1995; *Chen* et al., 2003; *Chen* and *Siebel*, 2004) and this suggests that a large quantity of material within the Variscan granitoids comes from reworking of older Precambrian, probably Proterozoic crust.

From the limited chemical variation it is evident that the Rinchnach and Patersdorf granites crystallized from moderately fractionated melts with little in situ fractional crystallization or assimilation processes. Major and trace element abundances are not compatible with the view that the granites are a differentiation product of the granodiorites. The difference in isotopic composition between the granodiorites and the granites is the strongest argument which excludes their consanguinity (Fig. 7). The granites and granodiorites as well as the palites have Sr and Nd isotopic compositions intermediate between mantle and crustal values. The presence of higher initial $^{87}Sr/^{86}Sr$ ratios and lower $\varepsilon Nd_{(t)}$ values in the granodiorites implies that these rocks originated from a more evolved source. The isotopic relationship is unique for granitoids from eastern Bavaria where the reverse relationship between dioritic and granitic rocks is normally observed (*Siebel* et al., 1997; *Chen* and *Siebel*, 2004). Granites and palites have similar εNd values but the latter have slightly more radiogenic $^{87}Sr/^{86}Sr$ ratios. Pfahl magmatism also produced dikes of granitic composition which cross-cut the palites. These dikes have the highest $^{87}Sr/^{86}Sr$ ratios and may not be co-genetic to the palites (for geochemical relation between palites and granitic dikes see *Siebel* et al., 2005). The diversity in petrographic, geochemical, and isotopic compositions of the Pfahl granitoids investigated so far suggests the presence of multiple, discrete magma

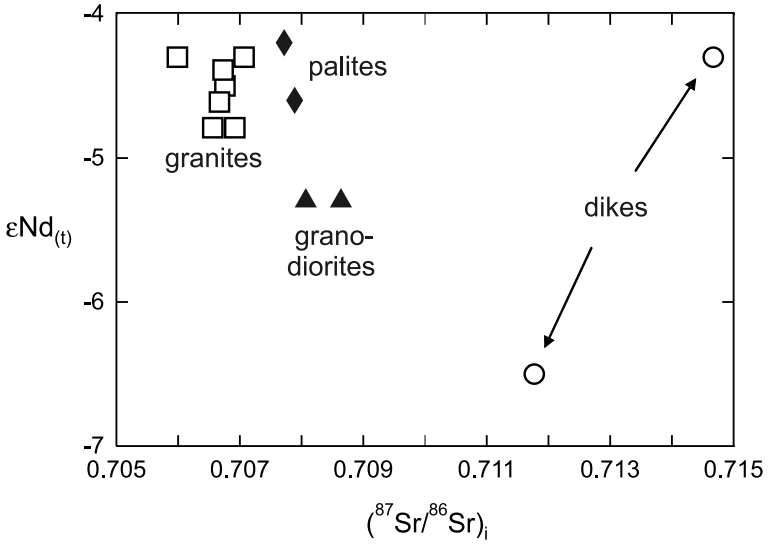

Fig. 7. εNd(t) versus initial $^{87}Sr/^{86}Sr$ diagram to characterize Pfahl granitoids from the Bavarian Forest. Granites and granodiorites investigated in this study. Data for palites and granitic dikes which crosscut the palites are from *Siebel* et al. (2005)

batches formed by crustal melting with some modification by addition of mantle material.

Inferences and conclusions

Magmatic rocks associated with the Bavarian Pfahl shear zone record a chronology of emplacement starting with the intrusion of palites (327–342 Ma), sheared granitic dikes (326–331 Ma) and continued with emplacement of granodiorites and granites (321–329 Ma). The radiometric data show that the shear zone was active during Visean-Namurian times. It seems likely that during magma transport from lower to upper crustal levels, the shear zone was used as a ramp or channel giving rise to the present distribution of the granitoids along the Pfahl zone. The Pfahl zone was active or reactivated after granite emplacement as shown by the fact that one of the granites is truncated by a mylonitic zone.

Although the geochronological data support a close temporal connection of granitic and granodioritic melts, from the chemical point of view the two granitoids have clearly different sources. The granites are less enriched in incompatible and REE elements and have higher ε_{Nd} and lower $^{87}Sr/^{86}Sr$ ratios than the granodiorites. This indicates the existence of two spatially separate and chemically different magma bodies within the crust. Given the inheritance of zircon cores in both types of granitoids it seems likely that both magmas contain significant amounts of material from Paleozoic igneous and older crustal precursors.

Acknowledgements

We thank *J. Rohrmüller* for assistance in the field. *G. Bartholomä*, *E. Reitter* and *H. Taubald* kindly helped us during the XRF and Sr–Nd isotope analyses. The text has benefited from the advices and thorough reviews by *F. Corfu* and *V. Janousek*.

References

Benisek A, Finger F (1993) Factors controlling the development of prism faces in granite zircons: a microprobe study. Contrib Mineral Petrol 114: 441–451

Brandmayr M, Dallmeyer RD, Handler R, Wallbrecher E (1995) Conjugate shear zones in the Southern Bohemian Massif (Austria): implications for Variscan and Alpine tectonothermal activity. Tectonophysics 248: 97–116

Chen F, Siebel W (2004) Zircon and titanite geochronology of the Fürstenstein granite massif, Bavarian Forest, NW Bohemian Massif: pulses of late Variscan magmatic activity. Eur J Mineral 16: 777–788

Chen F, Siebel W, Satir M (2003) Geochemical and isotopic composition and inherited zircon ages as evidence for lower crustal origin of two Variscan S-type granites in the NW Bohemian massif. Int J Earth Sci 92: 173–184

Corfu F, Hanchar JM, Hoskin PWO, Kinny P (2003) Atlas of zircon textures. In: *Hanchar JM, Hoskin PWO* (eds) Zircon. Rev Mineral Geochem 53: 469–500

Frentzel A (1911) Das Passauer Granitmassiv. Geognostisches Jahrb 24: 31 pp

Hanchar JM, Miller CF (1993) Zircon zonation patterns as revealed by cathodoluminescence and backscattered electron images: implications for interpretation of complex crustal histories. Chem Geol 110: 1–13

Hanchar JM, Rudnick RL (1995) Revealing hidden structures: the application of cathodoluminescence and back-scattered electron imaging to dating zircons from lower crustal xenoliths. Lithos 36: 289–303

Hofmann R (1962) Die Tektonik des Bayerischen Pfahls. Geol Rundsch 52: 332–346

Horn P, Köhler H, Müller-Sohnius D (1986) Rb–Sr Isotopengeochemie hydrothermaler Quarze des Bayerischen Pfahls und eines Flußspat-Schwerspat-Ganges von Nabburg-Wölsendorf/Bundesrepublik Deutschland. Chem Geol 58: 259–272

Kalt A, Berger A, Blümel P (1999) Metamorphic evolution of cordierite-bearing migmatites from the Bayerische Wald (Variscan belt, Germany). J Petrol 40: 601–627

Kalt A, Corfu F, Wijbrans JR (2000) Time calibration of a P-T path from a Variscan high-temperature low-pressure metamorphic complex (Bayerische Wald, Germany), and the detection of inherited monazite. Contrib Mineral Petrol 138: 143–163

Karabinos P (1997) An evaluation of the single-grain zircon evaporation method in highly discordant samples. Geochim Cosmochim Acta 61: 2467–2474

Kober B (1986) Whole-grain evaporation for $^{207}Pb/^{206}Pb$ age investigations on single zircons using a double-filament thermal ion source. Contrib Mineral Petrol 93: 481–490

Kober B (1987) Single-zircon evaporation combined with Pb^{+} emitter-bedding for $^{207}Pb/^{206}Pb$-age investigations using thermal ion mass spectrometry, and implications to zirconology. Contrib Mineral Petrol 96: 63–71

Köhler H (1970) Die Änderung der Zirkonmorphologie mit dem Differentiationsgrad eines Granits. N Jb Mineral Mh 9: 405–420

Krogh TE (1982) Improved accuracy of U–Pb zircon ages by the creation of more concordant systems using the air abrasion technique. Geochim Cosmochim Acta 46: 637–649

Liew TC, Hofmann AW (1988) Precambrian crustal components, plutonic associations, plate environment of the Hercynian fold belt of central Europe: indications from a Nd and Sr isotopic study. Contrib Mineral Petrol 98: 129–138

Ludwig KR (1993) PBDAT: a computer program for processing Pb–U–Th isotope data, version 1.2. USGS Open-file Report 88–542, 30 pp

Ludwig KR (2003) Isoplot 3.00 – a geochronological toolkit for Microsoft Excel. Berkeley Geochronology Center, Spec Publ No 4

Nasdala L, Zhang M, Kempe U, Panczer G, Gaft M, Andrut M, Plötze M (2003) Spectroscopic methods applied to zircon. In: *Hanchar JM, Hoskin PWO* (eds) Zircon. Rev Mineral Geochem 53: 427–467

Ochotzky H, Sandkühler B (1914) Zur Frage der Entstehung des Bayerischen Pfahles im Bayerischen Walde. Centralbl Mineral Geol Paläontol 1914: 190 pp

Ott WD (1983) Geologische Karte von Bayern, 1: 25 000, Blatt Nr. 6943, Viechtach. Bayer Geol Landesamt (Hrsg)

Peucker-Ehrenbrink B, Behr HJ (1993) Chemistry of hydrothermal quartz in the post-Variscan ''Bavarian Pfahl'' system, F.R. Germany. Chem Geol 103: 85–102

Potts PJ, Webb PC (1992) X-ray fluorescence spectrometry. J Geochem Expl 4: 251–296

Pupin JP (1980) Zircon and granite petrology. Contrib Mineral Petrol 73: 207–220

Siebel W, Höhndorf A, Wendt I (1995) Origin of late Variscan granitoids from NE Bavaria, Germany, exemplified by REE and Nd isotope systematics. Chem Geol 125: 249–270

Siebel W, Trzebski R, Stettner G, Hecht L, Casten U, Höhndorf A, Müller P (1997) Granitoid magmatism of the NW Bohemian Massif revealed: gravity data, composition, age relations and phase concept. Geol Rundsch 86: S45–S63

Siebel W, Chen F, Satir M (2003) Late-Variscan magmatism revisited: new implications from Pb-evaporation zircon ages on the emplacement of redwitzites and granites in NE Bavaria. Int J Earth Sci 92: 36–53

Siebel W, Blaha U, Chen F, Rohrmüller J (2005) Geochronology and geochemistry of a dyke-host rock association and implications for the formation of the Bavarian Pfahl shear zone, Bohemian Massif. Int J Earth Sci 94: 8–23

Söderlund U (1996) Conventional U–Pb dating versus single-grain Pb evaporation dating of complex zircons from a pegmatite in the high-grade gneisses of southwestern Sweden. Lithos 38: 93–105

Stacey JS, Kramers JD (1975) Approximation of terrestrial lead isotope evolution by a two stage model. Earth Planet Sci Lett 26: 207–221

Teipel U, Eichhorn R, Loth G, Rohrmüller J, Höll R, Kennedy A (2004) U–Pb SHRIMP and Nd isotopic data from the western Bohemian Massif (Bayerischer Wald, Germany): implications for Upper Vendian and Lower Ordovician magmatism. Int J Earth Sci 93: 782–801

Troll G (1967) Geologische Übersichtskarte des Bayerischen Waldes 1:100 000. Geol Bavarica 59 [Suppl]

Vavra G (1990) On the kinematics of zircon growth and its petrogenetic significance: a cathodoluminescence study. Contrib Mineral Petrol 106: 90–99

Vavra G (1994) Systematics of internal zircon morphology in major Variscan granitoid types. Contrib Mineral Petrol 117: 331–344

Authors' addresses: *W. Siebel* (corresponding author; e-mail: wolfgang.siebel@uni-tuebingen.de), and *M. Thiel*, Institut für Geowissenschaften, Universität Tübingen, Wilhelmstrasse 56, 72074 Tübingen, Germany; *F. Chen*, Laboratory for Radiogenic Isotope Geochemistry, Institute of Geology and Geophysics, Chinese Academy of Sciences, 100029 Beijing, China